LC-DET/2001-058
February 21, 2001

Si-W calorimeter performances

F. Badaud[2], JC. Brient[1], P. Cloarec[2], V. Djordjadze[3], P. Mora de Freitas[1], P. Gay[2], F. Le Diberder[4], S. Monteil[2], D. Orlando[1], D. Reid[5], H. Videau[1]

Abstract

The performances of the electromagnetic Si-W calorimeter with high granularity are reported. Reconstruction of isolated particles and jets, and particle identification are studied. The reconstruction of fully simulated jets leads to a preliminary resolution about $35\%/\sqrt{\mathrm{E_{jet}}}$ for the ENERGY FLOW algorithm. An illustration of the performances based on typical physics processes of interest at the energy scale of the TESLA fascility is also indicated.

[1]LPNHE, Ecole Polytechnique, $IN^2P^3 - CNRS$, 91128 Palaiseau, France.
[2]LPC, Univ. Blaise Pascal, $IN^2P^3 - CNRS$, 63177 Aubière, France.
[3]DESY-Zeuthen, 15735 Zeuthen, Germany.
[4]LPNHE, Univ. Paris VI-VII, $IN^2P^3 - CNRS$, 75252 Paris, France.
[5]NIKHEF, 1009 DB Amsterdam, The Netherlands.

1 Introduction

In order to perform high precision measurements as well as search for new phenomena at a next Linear Collider, excellent ENERGY FLOW performances are mandatory. A particular emphasis is given about both the electromagnetic and hadronic calorimetry. Some of the performances reported in this Note are obtained thanks to the combination of electromagnetic and hadronic calorimeters with informations from tracking system.

The electromagnetic calorimeter (ECAL) under consideration is a Silicon/Tungsten sampling calorimeter. It is characterized by a high granularity design with elementary detection cell consisting in 1x1 cm^2 silicon pad and it is longitudinally segmented in 40 layers, covering 24 X_0. Details about the full design of the ECAL are given in Ref. [1].

The ECAL is simulated with GEANT.4 [2] according to two geometries so-called LINEAIRE and MOKKA hereafter. In the LINEAIRE version, the silicon pads and the radiator are assumed to be on concentric cylinders around the beam axis. The tungsten pads are assembled such that they form projective towers pointing to the centre-of-gravity of the detector. This version was intended to test the relevance of the detector choice by evaluating the intrinsic performances of the detector and the related ideas about particles reconstruction. A complete simulation of the actual design of the detector, MOKKA, is consequently developed, in order to quantify in a more realistic way the calorimeter performances. The simulation takes into account the construction in several modules both in the barrel and end-caps parts and reflects the pad assembly in each module, including the overlap between the modules. The software simulation is detailed in Ref. [3]. A 4 T axial magnetic field is assumed in all the simulations used throughout this Note. In order to take into account the zero suppression from the electronics, every pad with an energy deposition less than 100 keV is removed from the fired pad collection.

The hadronic calorimeter (HCAL) involved in this study is described in Ref. [1]. It is a stack of 40 tungsten/tube sandwiches and the readout allows a 3D reconstruction of the information.

This document reports the main performances of the Si/W ECAL in combination with the 3D-HCAL. The intrinsic performances of the ECAL are quickly reported in Section 2. Two complementary approaches of the photon reconstruction are described in Section 3. Section 4 is devoted to the neutral hadron identification. The identification of the charged leptons, electrons and muons, is discussed in Sections 5 and 6. Performances in terms of efficiencies and misidentification probabilities are obtained with benchmark test samples : $\pi^{\pm}/\gamma$, $\pi^{\pm}/K^0$ and $\pi^{\pm}/\mu$ and relevant processes such as muons in b-jets and tau decays. The impact on jet reconstruction is reported in Section 7 followed by the illustration with some physics processes : higgs boson decays in two photons, ZZ (WW) collisions and $e^+e^- \rightarrow hhZ$. The latter studies are reported in Section 8.

2 Intrinsic performances of the ECAL

Single photons with different energies interacting in the ECAL have been simulated. The energy of the photons is varied from 200 MeV up to 15 GeV and each sample consists in approximately one thousand of events for each energy.

The raw energies deposited in the silicon cells (pads) are summed up and corrected to yield the measured photon energy :

$$E_\gamma \text{ (GeV)} = \alpha(\sum_{i=1}^{30} E_i(\text{MeV}) + 1.4 \sum_{i=31}^{40} E_i(\text{MeV}) ,$$

where i represents the silicon cell layer and α a parameter depending upon the selection of the cells ($\alpha = 0.03125$ when no selection is made). The following energy resolution has been derived :

$$\frac{\sigma_E}{E} = \frac{10.3\%}{\sqrt{E}} + 1\% .$$

It has been observed that the energy resolution does not depend, to a first approximation, on the polar angle. With the same events, the photon direction is reconstructed by a fit with a straight line to the energy barycentra of the electromagnetic shower distribution, measured for each layer. The angular resolution on the reconstructed photon direction is found to be of the order of 20 mrad.

3 Photon reconstruction

To perform the photon reconstruction, two approaches are followed. The first one, used as the standard and denoted Photon-Finder algorithm (PFD), is based on a purely geometrical clustering while an alternative attempt (EMILE) uses a probability concept. EMILE stands for Energy Measurement Intended for Low Electromagnetic showers.

3.1 Photon-Finder

The algorithm acts in two steps. The first part consists in the determination of the seed of the electromagnetic shower, operated after a 'track deletion' (TD) : the entry point positions of photon candidates are established and every pad within one centimeter to the extrapolation of any charged track is not taken into account. Afterwards, the clusterisation of the pads is performed from those seeds according to spatial proximity rules.

In details, the information collected on the first ten layers of the ECAL are summed up in order to form a virtual stack. The virtual pads, accordingly constructed are ranked in decreasing energy order. As soon as a pad is not a neighbour of the previous virtual pad in ordered list, this pad is the seed of a new cluster.

Around this seed, the real pads are clustered iteratively. To deal with the non-projective geometry version, the neighbouring rule between two pads is based on an equivalent distance. This is the distance between the projections on the entrance plan towards the centre of the detector of the cluster's centre-of-gravity and the pad position.

Fired pads with an equivalent distance to the cluster less than one centimeter belong to the cluster. Some unassociated pads are recovered according to the angle between the direction of the pad position and the centre-of-gravity of the cluster.

3.1.1 Performances

To test the performances of the algorithm, samples of isolated photons with energy from 150 MeV up to 100 GeV have been simulated with the MOKKA geometry of the ECAL. The clustering efficiency and the fraction of recovered electromagnetic energy are displayed on Fig. 1.

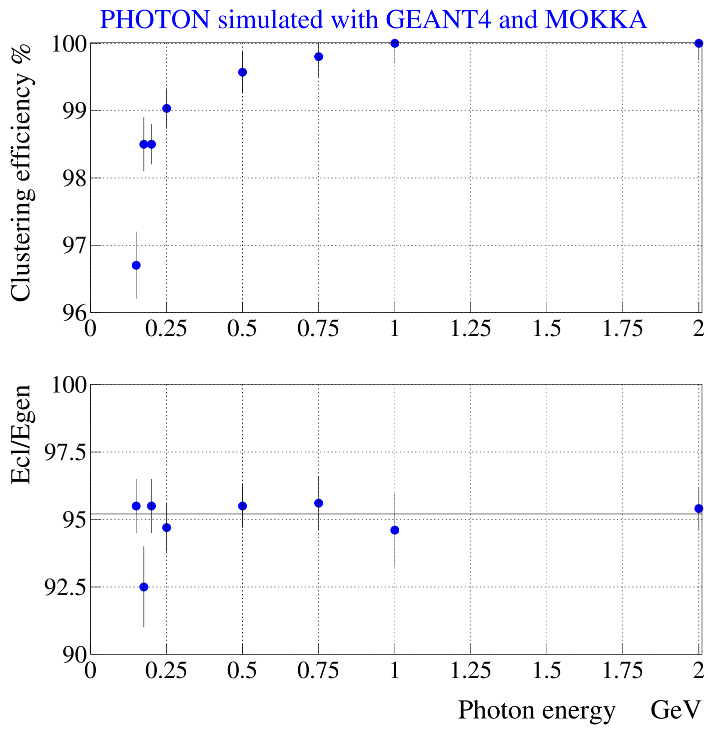

Figure 1: *Clustering efficiency (a) and fraction of recovered electromagnetic energy (b) as a function of the photon energy with PFD algorithm.*

The efficiency to find a photon is greater than 99% when the photon energy is above 250 MeV and remains greater than 96% even with low energy photon (150 MeV). The rate of fake electromagnetic clusters created by a fluctuation of an electromagnetic shower is about few per mil : from 4.10^{-3} up to 9.10^{-3} for photon energy of 500 MeV and 100 GeV respectively. The fraction of the total energy in the cluster is stable and about 95% up to four GeV and slowly increases up to 99.5% at 100 GeV.

The energy and angular resolution after clustering are displayed on Figs. 2 and 3. The stochastic term is $11\%/\sqrt{\mathrm{E(GeV)}}$ up to few GeV and then about $13.7\%/\sqrt{\mathrm{E(GeV)}}$, while the angular resolution $\delta\theta$ is $\delta\theta(\mathrm{mrad}){=}0.63/\sqrt{\mathrm{E(GeV)}}{+}0.24$ for photon energy down to few hundred MeV.

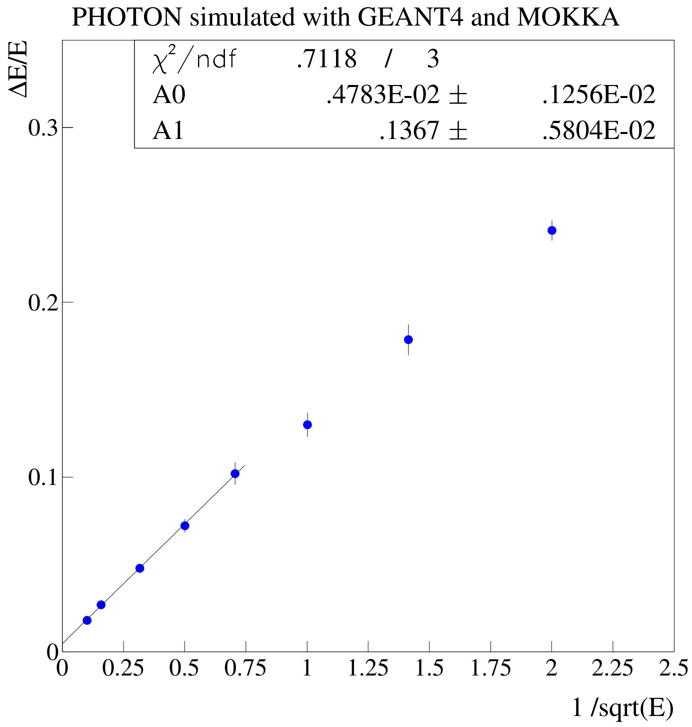

Figure 2: *Energy resolution as a function of the photon energy with PFD algorithm*

3.2 An alternative attempt for photon reconstruction

The EMILE approach acts essentially on the reconstruction of photons interacting close to a charged hadron in the ECAL as well as the reconstruction of very low energy photons [4].

Principles and D_{ij} definition

The leading idea is to correlate the pads according to some physical insight of an electromagnetic shower. Thus, a probability D_{ij} that a pad j is related to a pad i (with $i < j$, *i.e.* following the development of the shower) is defined as : $D_{ij} = \dfrac{d_{ij}}{\sum_i d_{ij}}$, where $d_{ij} = e^{\frac{-\rho_{i,j}}{X_0}} \times \dfrac{1}{1 - \beta cos\theta_{ij}} \times \dfrac{1}{\chi_E}$;

$\rho_{i,j}$ is the distance between the pads and X_0 is the mean radiation length of the detector.

The factor $e^{\frac{-\rho_{i,j}}{X_0}}$ ensures the long distance processes which occur in the development of the shower to be accounted for.

θ_{ij} is the angle formed by the vectors $\vec{\rho}_{i,j}$ and $\vec{\rho}_{IP,i}$, where $\rho_{IP,i}$ stands for the distance of the pad i to the interaction point IP. β is a parameter defined analogously to the velocity of the electrons in the bremsstrahlung process; it has been adjusted to 0.99. The term $\dfrac{1}{1 - \beta cos\theta_{ij}}$ is intended to model the angular spread of the shower.

χ_E represents an estimator of the energy relationship between the pads i and j. It is defined as the likelihood for a pair of pad (i, j) to follow the longitudinal energy deposit profile of low energy photons.

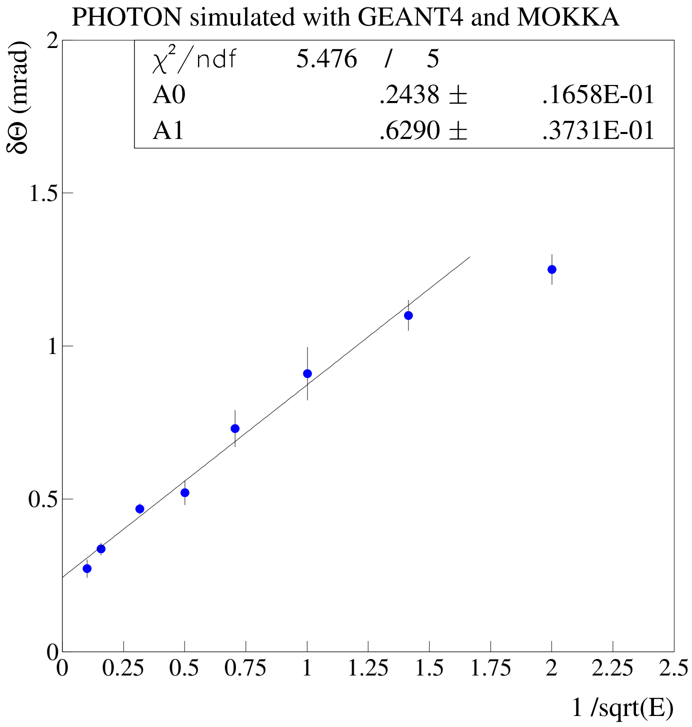

Figure 3: *Angular resolution as a function of the photon energy with PFD algorithm*

3.2.1 Photon reconstruction

The energy of the pad j is distributed to the pad i weighted by the probability D_{ij}, starting from the latest layer of the ECAL. The electromagnetic shower is then "rewinded" until all pads j, with $D_{ij} = 0$ whatever i is, are found, as illustrated Fig. 4. They are defined as the roots of the shower. By construction, it may happen that several roots are found for a single photon. For instance, the D_{ij} is zero for two adjacent pads on the same layer.

Two criteria are defined to merge the roots :

- the distance between two root pads a and b, less than 1.7 cm,
- the distance between the two energy barycentra corresponding to the root pads a and b must be less than 0.5 cm.

These barycentra are obtained by propagating at each step of the procedure the position of the pad j weighted by its energy. The merging procedure is 100 % efficient. The algorithm provides a root pad, to which is assigned the position of the first interaction, the position of the shower energy barycenter and the shower energy.

3.2.2 Tests of the procedure and performances

The ability of the algorithm to reconstruct photons is tested with single photons in energy range from 100 MeV to 15 GeV. Figure 5 displays the fraction of energy reconstructed as a

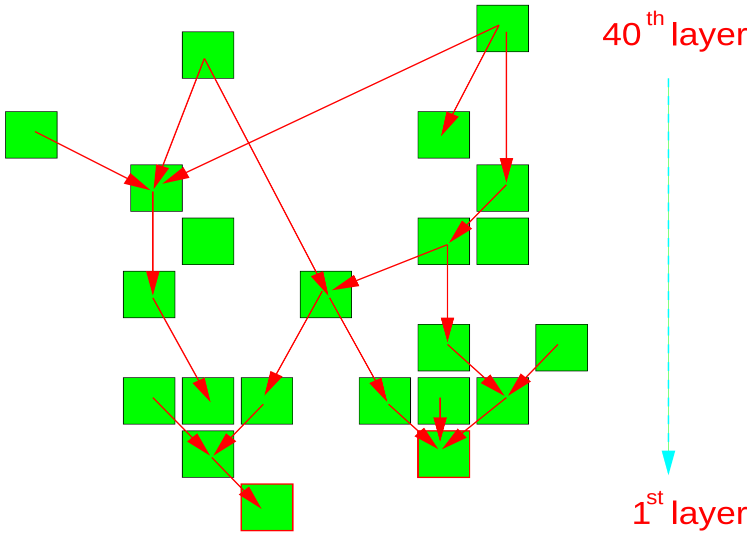

Figure 4: *Energy distribution from the outer pads to the root candidates. Energy is deposited on all innerer pads with $D_{ij} \neq 0$, weighted according to their D_{ij} value.*

function of the photon energy. Excellent performances are obtained, even for very low energy photons.

As a corollary, the energy resolution is close to the intrinsic one,

$$\frac{\sigma_E}{E} = \frac{11\%}{\sqrt{E}} + 1\% \ .$$

3.3 $\gamma/\pi^{\pm}$separation

The most relevant test of the algorithms (PFD and EMILE) ability to reconstruct photons for the energy flow purpose is to search for an electromagnetic shower close to the interaction of a charged hadron in the ECAL.

The PFD algorithm has been tested with a sample of ρ decays issued from τ decays. The photon reconstruction efficiency is reported in Fig. 6 as a function of the distance to the charged track at the entrance of the ECAL.

The root of the hadronic shower, when occurring in the ECAL, is reconstructed from energy deposition considerations. The pads which are found above the root belonging to a 15 degrees cone for which the top is the root are removed.

The EMILE algorithm is tested by considering a 10 GeV charged pion and a 1 GeV photon generated with the LINEAIRE simulation version, entering the ECAL at 1, 2, 3 and 4 cm distances, respectively.

The photon reconstruction efficiencies, without any treatment of the hadronic shower are displayed on the first line of the Table 1. No photon identification is performed at this stage; only the root carrying more than 50 % of the simulated energy deposited by the photon is considered.

When adding informations from the π^+ trajectory and a reconstruction of the hadronic root, the related efficiencies reported on the third line of Table 1, are obtained.

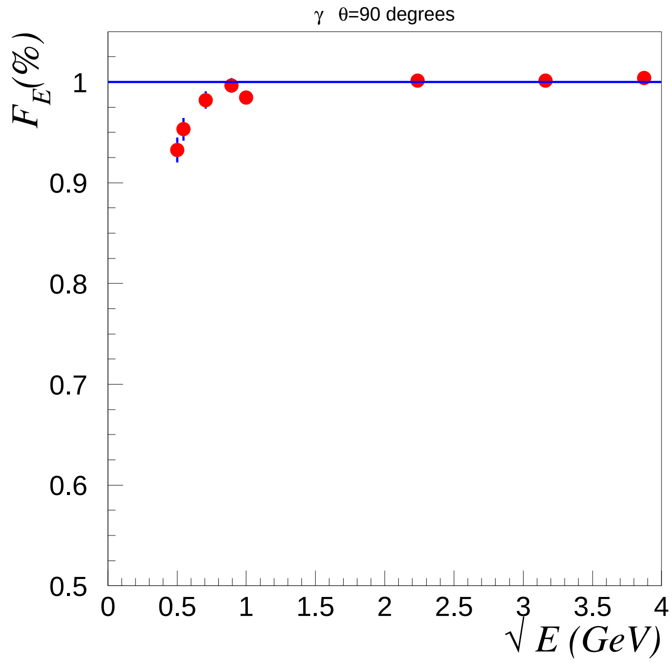

Figure 5: *Fraction of reconstructed energy as a function of the square root of the generated true photon energy .*

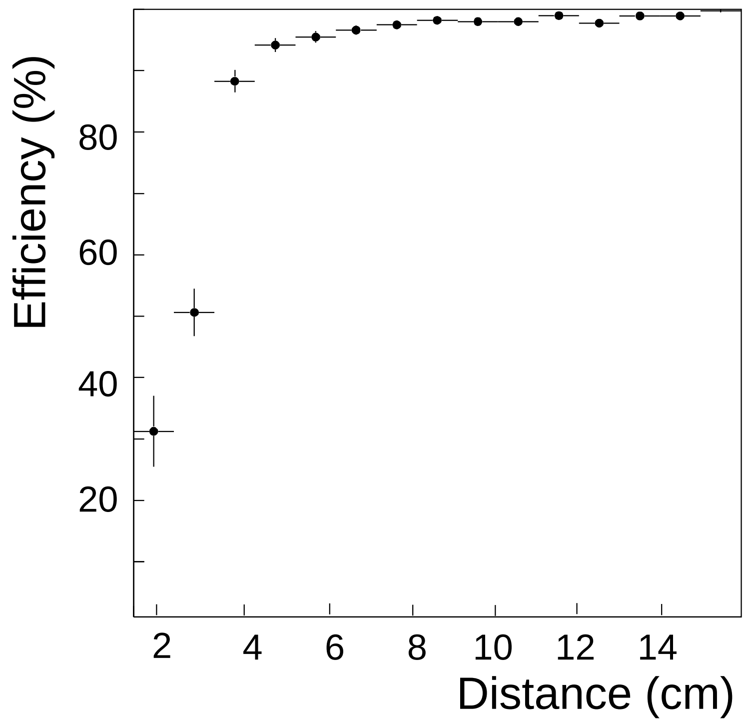

Figure 6: *Photon reconstruction efficiency as a function of the distance to the charged track with PFD algorithm.*

π^+/γ distances	2 cm	3 cm	4 cm
D_{ij}	21%	53 %	80 %
D_{ij} + TD	47%	61 %	90 %
D_{ij} + hadronic shower	67%	84 %	95 %

Table 1: *Reconstruction efficiencies results for three samples of photons generated at 2, 3 and 4 cm distances to a charged pion in the ECAL. TD (standing for Track Deletion) means that the pads closer than one centimeter to the extrapolation of the π^+ trajectory are removed, prior to the photon reconstruction procedure. The third line of the Table displays the efficiencies obtained when considering hadronic shower informations.*

Excellent performances are obtained in the photon reconstruction PFD when considering distances larger than few centimeters. Further improvements are obtained with the EMILE approach when considering photons very close to a charged hadron.

3.4 Summary and prospects

EMILE is an algorithm intended to reconstruct low energy photons produced close to hadrons in the ECAL detector. Based on a probabilistic distribution of the pad energies toward a pad root, following the physical insight of an electromagnetic shower, EMILE is found to be an adequate tool for the Energy Flow purpose and a promising complementary approach to the Photon-Finder algorithm.

Developments of the algorithm are needed to evaluate in a complete way its performances in terms of hadron misidentification for instance, such that analyses of simulated physics events can be envisaged.

4 Neutral hadron reconstruction

The present approach to cluster neutral hadrons is based on a fuzzy inference [5] using the distance between two hits. The choice of a fuzzy technique is guided by the fact that pads may often be hit by several particles. This is the first part of the reconstruction method followed by an association of the clusters and a treatment event by event.

4.1 Reconstruction procedure

Clusterisation

The first step in building up the fuzzy inference scheme is to analyze simulated events in order to find the distributions of distances and angles between hits associated to the same particle, from which probability distributions are derived. About 2 10^4 events are used for that purpose : 4500 K^0, 4500 π^-, 10^4 couples π^-, K^0.

The *possibility* distributions π_i are given by the following relation

$$\pi_i = \sum_{j=1}^{n} \min\left(p_i, p_j\right)$$

where p_i is the probability of the distance d_i or angle ϑ_i.

Both angle and distance informations are used to build an inference scheme with four membership functions based on the possibility distributions. Basically, for any given couple of hits, a degree of membership to the same cluster is given by the probability of finding or not these distance and angle in a "true" cluster; a certain degree of non–membership is obtained similarly.

Two couples of hits (a and b) belong to a given cluster according the following rules :

1. if the distance between a and b is likely to be found in a given cluster *AND* if the angle between them fulfills this condition too, then they belong to the same cluster;

2. if the distance between a and b is not likely to be found in a given cluster *OR* if the angle between them is not, then they do not belong to the same cluster.

Using this algorithm recursively, a cluster is built up by joining all the hits for which the degree of membership to the same cluster is greater than the degree of non–membership. In addition, a parameter is introduced to weight the importance of the two rules.

Association of clusters

After this first step, approximately 25 clusters are found per event that need to be linked together. The merging procedure is based on a small number of variables related to the cluster : the center of gravity, the direction, evaluated as the variance in the three spatial directions and the position of the closest and farest hits. Two clusters are considered part of the same object if the following conditions are fulfilled :

1. the distance between the two centers of gravity is less than 20 cm,

2. the distance between the center of gravity of the first cluster and the direction of the other one is less than 7 cm,

3. the distance between the closest points belonging to the two considered clusters is less than 1.5 cm,

4. the angle between the two directions is less than 0.15 rad

5. the distance between the two directions is less than 7 cm and they do not point to the origin.

Event by event treatment

Reconstruction can be improved by adjusting the weight parameter for the two rules on an event by event basis. 15 different values of the weight are considered leading to 15 different reconstructions. The best one is chosen according to an inference scheme using the three membership functions for each cluster to the set of "true clusters", "fakes" and "wrong clusters" (*i.e.* the cases in which the two clusters where recognized as one); they are based on both the mean distance between hits in the recognized cluster and charged particle momentum given by the tracking system.
To each cluster is then associated a probability it has to be a "true" cluster. The best reconstruction is chosen according to the greatest probability.

4.2 Performances

Neutral hadrons identification performances have been derived from the study of K^* decays. Thus, the source of K^0 and π^- event consists in about 5000 K^* decays simulated events. A good reconstruction of an event is assumed when at least two clusters are found, one of which being the π^- and the others made of pads hit by the K^0. A cluster is classified as fake if made up by more than 50% pads hit by the π^-. Figure 7 shows the reconstruction efficiency, as a function of distance from the charged hadron.

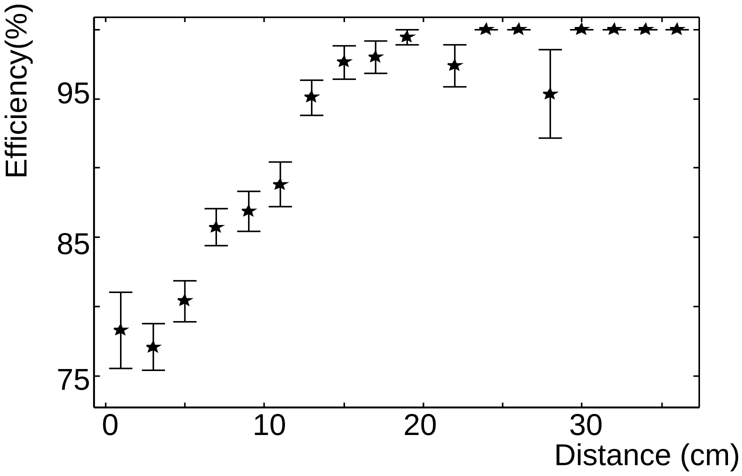

Figure 7: *Neutral hadron efficiency as a function of distance from the charged hadron*

A comforting 87.1% total efficiency is found, and in particular an efficiency between 75% and 85% at distances less than 10 cm. For distances over 20 cm the efficiency is almost 100% as expected.

Figure 8 shows the efficiency as a function of the energy of the two particles. There is a strong dependence on the charged particle energy (that reasonably masks the other one when very energetic), while the efficiency is almost the same whatever the K^0 energy is. This may suggest the use of different parameters or algorithms utilizing in a better way the π energy, that can be easily and accurately measured by the tracking system. In other hand, low–energy neutral particles still need to be studied.

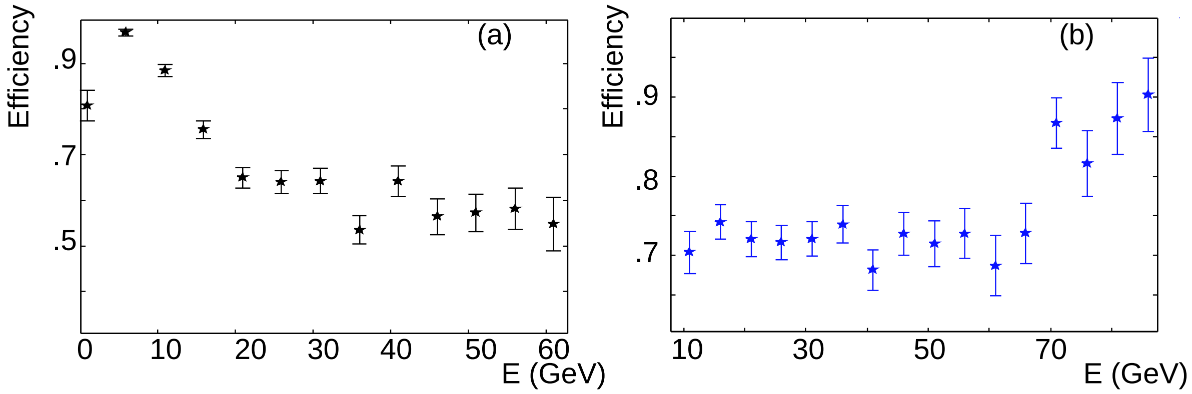

Figure 8: *Neutral hadron efficiency as a function of the (a) π and (b) K^0 energy.*

A sample of π^- is used in order to test the fake rate generated by the reconstruction. The only imposed limit is an energy cut at 500 MeV. Figure 9 displays the fake rate as a function of the π^- energy. As expected, the number of fakes is very low, in particular for relatively low energy pions (*i.e.* under 20 GeV).

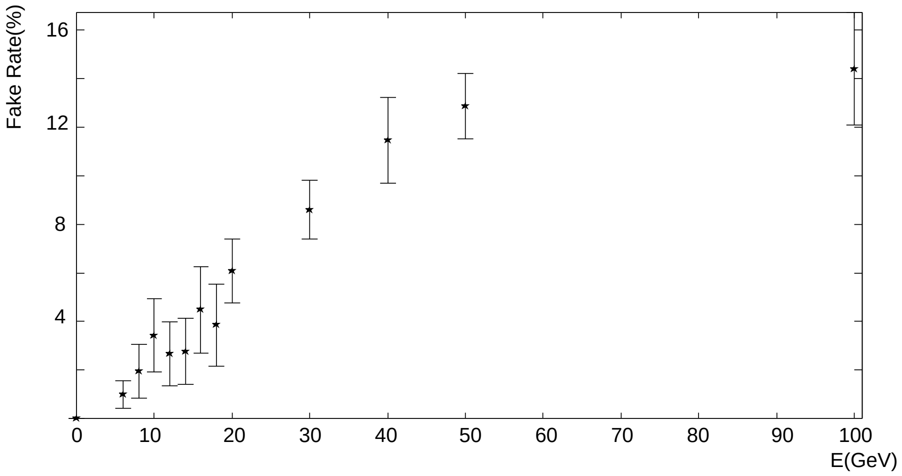

Figure 9: *Percentage of fakes as a function of the π^- energy*

Sources	Id. as electron	Id. as hadron
isolated electron	99.82 $\pm$ 0.08 %	2.2 10^{-3}
isolated pion	2.1 $\pm$ 2.1 10^{-4}	99.98 %
$\tau \to \rho\nu$	8.1 $\pm$ 8.1 10^{-5}	99.99 %
both pions	1.2 $\pm$ 0.8 10^{-4}	99.99 %

Table 2: *charged track electron/hadron separation.*

5 Electron identification

An electron identification is developed from a sample of about 2700 electrons. Electrons are generated randomly from 2 to 50 GeV/c, by considering flat polar and azimuthal angles distributions. In order to derive misidentification rates, a sample of charged hadrons are generated from hadronic τ decays $\tau \to \pi^{\pm}\nu$ (4700 events) or $\tau \to \rho^{\pm}\nu$ (12500 events).

The electron identification is built on a likelihood estimator technique. The estimator combines the following variables :

- the energy along the track extrapolation of the 4 closest pads (4 'central towers'), normalized to the electron momentum ($\|\vec{P}\|$), denoted E_4,
- E_4 - $\|\vec{P}\|$ normalized to the expected error,
- $E_4 + E_\gamma$ where E_γ is the photon(s) energy reconstructed in the 16 'central-towers', normalized to the track momentum (recovery of the bremsstrahlung),
- the depth of the beginning of the shower,
- the mean depth of the shower, among the 4-central towers (track momentum dependence is taken into account).

In order to account for the track momentum dependence of the variables, as far as the charged hadrons are concerned, five subsamples are considered : 2-5 , 5-10 , 10-15, 15-20 and above 20 GeV/c. Reference distributions in the likelihood estimator construction are taken independently for each subsample. Figure 10 shows the reference distributions for some of the variables used in the estimator for $\|\vec{P}\| > 5$GeV/c. The estimator response in the same momentum region is displayed on Fig. 11.

Performances of the electron identification obtained for a cut at 0.5 in the estimator distribution are summarized in Table 2. Excellent electron identification efficiency is achieved with a very small hadron misidentification, of the order of 10^{-4}, indicating that electron/hadron separation is not so far from perfect. This result is a further illustration of the potential of the Si/W ECAL under consideration.

6 Muon Identification

The ECAL and HCAL were simulated with the MOKKA geometry. Six samples of 1000 single pions (muons) with momenta of 2, 3, 4, 5, 10 and 50 GeV/c have been generated. The particles

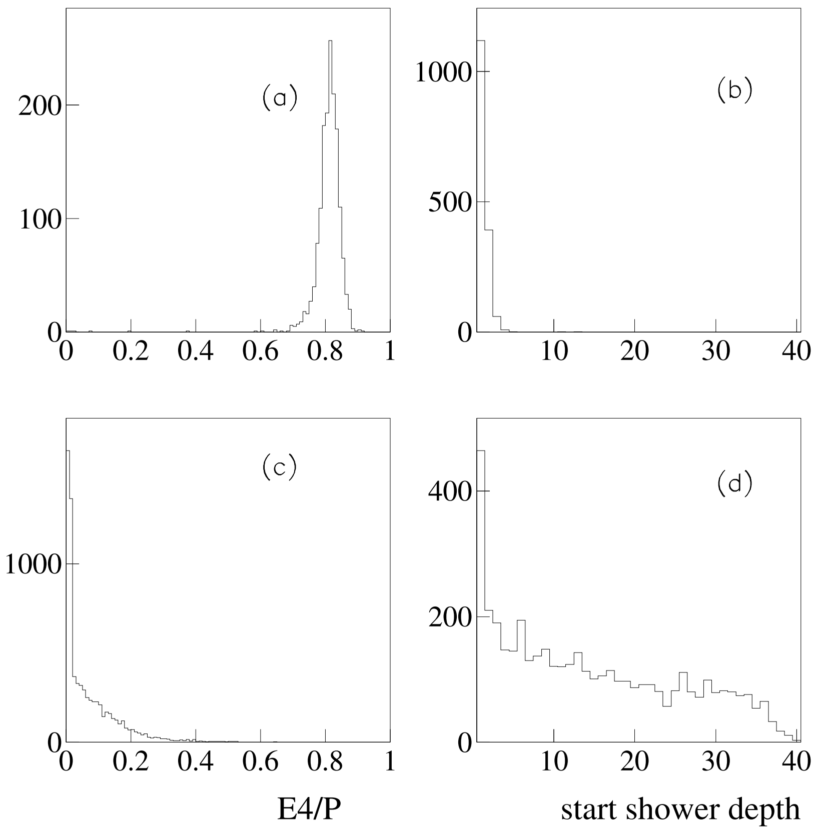

Figure 10: *Distributions of the variables used in the estimator for* $\|\vec{P}\| > 5$ GeV/c*. Figures (a) and (b) are for the electrons, figures (c) and (d) for the charged pions in the* $\tau \to \rho\nu$ *decays.*

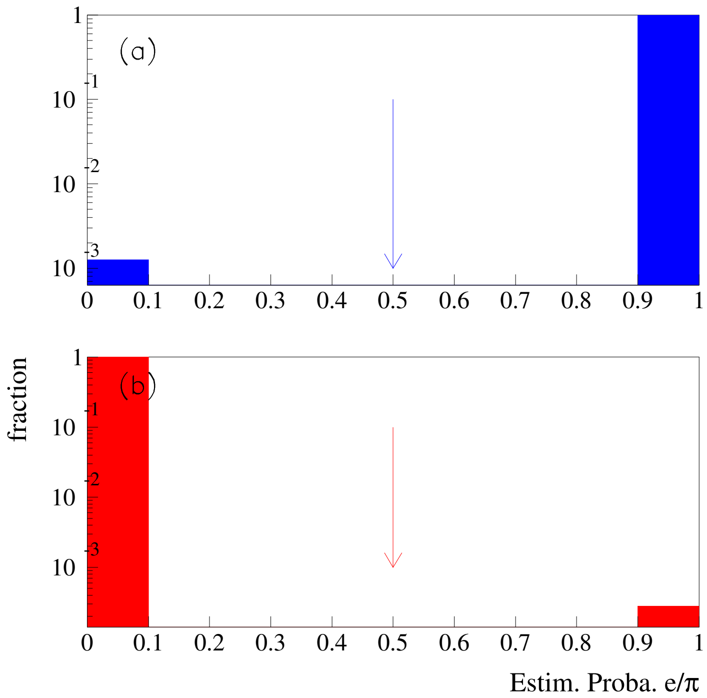

Figure 11: *Estimator response for* $P > 5$ GeV/c *tracks : (a) electrons, (b) charged pions in the* $\tau \to \rho\nu$ *decays. The arrow shows the position of the cut used to identify electrons.*

are produced with a flat spectrum in the barrel part of the detector : $0<\phi< 2\pi$ and $0.87<\theta<2.27$ where ϕ and θ are the azimuthal and polar angle. In order to study muons in a jet environment, 1500 events produced in $e^+e^-\rightarrow Z/\gamma\rightarrow b\bar{b}$ events are used. A centre-of-mass energy of 500 GeV is considered, the polar angular region is restricted to the barrel part and no cut on the muon momentum is applied.

The reconstruction of the muons (pions) in the calorimeters consists of two main steps. First, an association of the pads with the trajectory is performed and secondly, the shower tail transverse profile is estimated.

In the first part, assuming a perfect reconstruction of the trajectory by the tracking system, the helix is extrapolated to the inner face of the ECAL. The first fired pad within one centimeter on r-ϕ-z cylinder along the track extrapolation is considered as the first hit cell. The collection of the next pads is performed step by step looking for hits within a search road along the helix track extrapolation taking into account the multiple scattering. Since no energy cuts are required, this procedure is entirely digital. The pads selected with this procedure forms the "calorimeter-track".

The transverse profile estimator (TPE) is then defined as the RMS of the transverse distance of all the collected hits around the helix extrapolation, lying on the last 20 cm of the "calorimeter-track". The TPE is also entirely digital.

For high energy muons (namely momenta above 5 GeV/c), the rejection of pions is achieved by requiring the last measured point on the 'calorimeter-track' to be in the last two layers of the HCAL. However for 50 GeV/c, there is a fairly serious contamination from pions, which decreases accordingly with momenta. The case of muon candidates of about four GeV/c momentum represents the easiest situation : all muons reach the outside of the HCAL and, the pions showers stop before. There is therefore no need for a cut on the TPE.

The transverse profile estimator (TPE) and the position of the last point attached to the "calorimeter-track" are combined into a single variable.

Efficiencies and probabilities of misidentifying a pion as a muon as a function of its momentum are reported Table 3.

muon efficiency	misidentification				
	Momentum (GeV/c)				
	50	10	5	4	3
80%	0.4%	0.5%	0.8 %	0.3%	0.9%
90%	0.4%	0.8%	1.3%	0.5%	1.1%
95 %	0.5%	0.8%	1.3 %	0.9%	1.6%

Table 3: *Probability of misidentifying a pion as a muon as a function of its momentum and muon efficiency for the two variables NN.*

A second attempt is realised by considering the set of the four following variables again combined in a single discriminant variable : the position of the last point attached to the "calorimeter-track", $\sin(\theta_{track})$, the "calorimeter-track" length, the product TPE$\times\sqrt{P_{track}}$, where θ_{track} and P_{track} are the polar angle of the track and its momentum respectively. The analysis sample consists in a mixture of 4, 5, 10 and 50 GeV/c candidates. Improved results are obtained. For example, the misidentification probability at 4 GeV/c is 9% instead of 29.1% for a muon efficiency of 99%.

As there is a changeover in the behaviour of the TPE variable going from exiting to stopping muons, the 3 GeV/c sample can not be easily trained simultaneously. Samples defined by transverse momentum rather then momentum istself may yield cleaner results.

Since low P_t muons (namely $P_t \leq 3$ GeV/c) stop in the calorimeters, different NNs are trained with 2 and 3 GeV/c samples. Three input variables are used : $\|\cos(\theta_{track})\|$, TPE and the 'calorimeter-track' length. The obtained performances are reported in Table 4.

muon efficiency	misidentification	
	Momentum (GeV/c)	
	3	2
80%	0.9%	2.1%
90%	0.9%	4.5%
95%	1.5%	8.9%

Table 4: *Probability of misidentifying a soft pion as a muon as a function of the muon efficiency fo the three-variables NN.*

In summary, isolated pions with momentum from 3 GeV/c show a misidentification at the level of 0.3 - 0.9%, for a muon efficiency of 80%. When considering an efficiency of 95%, a misidentification from 0.4 to 1.5% is observed. The two GeV/c region is significantly worse and requires a dedicated procedure.

Muon identification performances have been looked in jet environnement with cut analyses.

momentum range	efficiency	misidentification
>6 GeV/c	81%	1.1%
5-6 GeV/c	84%	1.3%
4-5 GeV/c	91%	1.1%
3-4 GeV/c	83%	1.7%
2-3 GeV/c	85%	1.6%
1-2 GeV/c	49%	3.8%

Table 5: *Efficiencies and misidentification of muons in b jets according momenta range.*

It appears that an efficiency of 80-92% is reachable from 2 GeV upwards with about 1.1 to 1.7% pion misidentification rate. Performances are summarised Table 5.

6.1 Prospectives

The pattern recognition reported in this note is simple and does not use energy depositions in the calorimeters. It has been tuned on isolated tracks and should be improved for jets. For instance, the reconstruction could be designed as a function of the isolation of the track and the track fit with the points associated in the calorimeter could be implemented. A dedicated study the low momenta region, namely one to three GeV/c, will lead to improvements.

7 Jet reconstruction

Z decays in two jets events at a centre-of-mass energy of 91.2 GeV have been simulated with MOKKA geometry for both ECAL and 3D-HCAL. The jet energy measurement is based on an analytic ENERGY FLOW algorithm where the reconstruction of the photons and the neutral hadrons are performed with methods developed in the previous Sections; the charged particles are measured with the TPC. The obtained results are displayed on Fig. 12 where a 3.1 GeV/c^2 resolution on the visible jet energy is obtained.

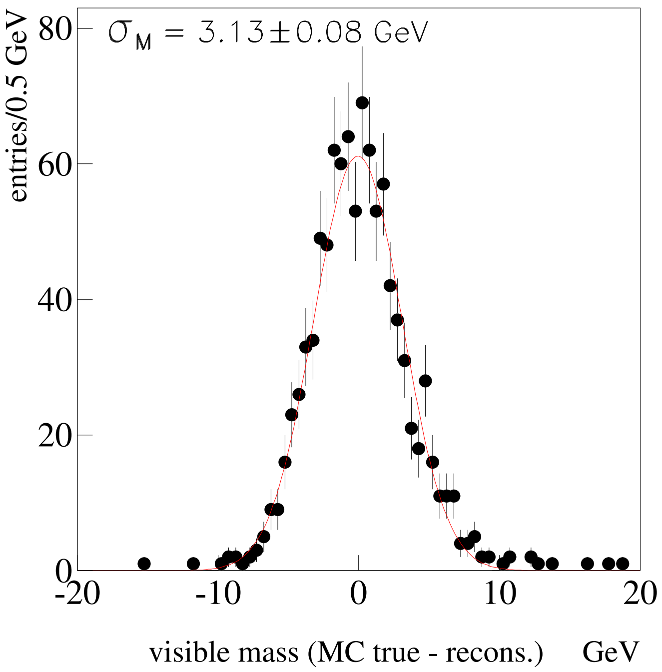

Figure 12: *Distribution of the variation of the reconstructed visible mass with respect to the true one* (ΔM) *in Z$\rightarrow$q$\bar{\text{q}}$ events at $\sqrt{\text{s}}$=91.2 GeV*

It has been shown that the result of the full simulation is reproduced by a fast-simulation if such a modelisation takes into account the efficiency reconstruction, energy and direction resolutions of the photons or neutral hadrons as a function of energy, distance to the charged hadron and the corresponding fake rate. A quasi-full reconstruction, consisting in the full reconstruction except for neutral hadrons (treated as in the fast-simulation) is used to derive the expected resolution on visible masses for some other jet samples. The comparison with a typical LEP detector is displayed on Fig. 13; the improvement is clearly observable. At $\sqrt{\text{s}}$=91.2 GeV, the difference between the visible mass resolution obtained with the full- and quasi-full reconstructions is around 100 MeV.

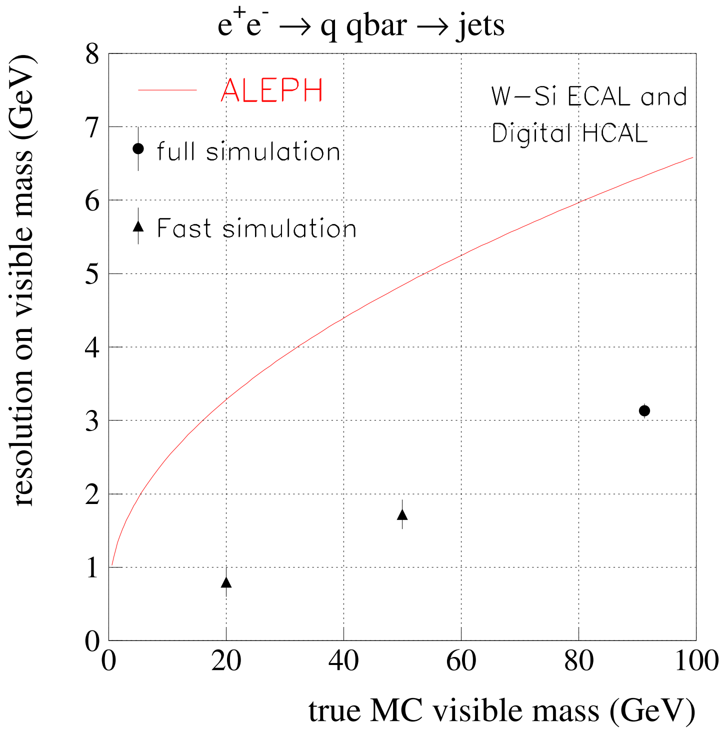

Figure 13: *Resolution on the visible mass as a function of the visible mass obtained with a quasi-full reconstruction of the jets in high granularity calorimeters (TESLA); results obtained with the LEP-detector (ALEPH) are also indicated for comparison.*

8 Calorimeter performances with Physics processes

The immediate test of the ECAL consists in reconstructing the Higgs boson mass through the analysis of the process $H \to \gamma\gamma$. The reconstruction of the jets in ZZ and WW collisions are tested too, and the impact of the ENERGY FLOW is evaluated in $e^+e^- \to hhZ$ process.

$H \to \gamma\gamma$ analysis

The event sample consists in 300 $e^+e^- \to HZ$ events where $H \to \gamma\gamma$, simulated with PYTHIA 5.7 [6] generator at a centre-of-mass energy of 500 GeV and for m_H=120 GeV/c^2. To estimate the Si-W ECAL performance for Higgs detection into two γ a full electromagnetic shower simulation into the ECAL is performed. The TESLA detector is simulated with BRAHMS [7] based on GEANT3 [8]. Figure 14 illustrates the electromagnetic shower development of the two photons into the ECAL.

A simple clustering method based on vicinity rules between pads is used. Among all the clusters, only the two most energetic ones which do not match a charged track are used in the mass reconstruction. When a cluster is found at the border of two modules, the closest cluster is merged with it if its energy deposition is greater than one GeV. The cluster direction is obtained from the energy weighted centre-of-gravity of the cluster and the interaction point.

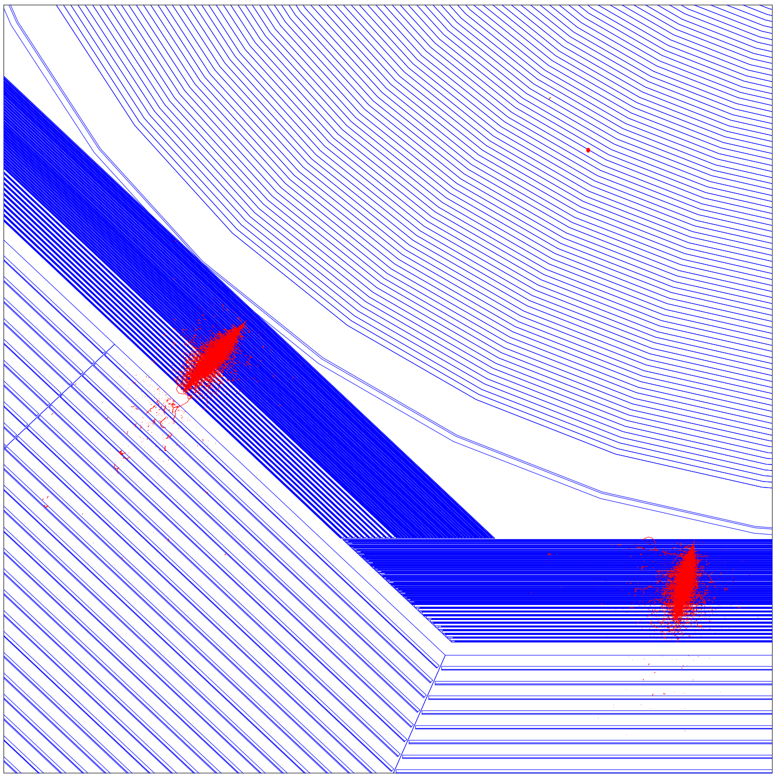

Figure 14: *A transverse view of a* $H \to \gamma\gamma$ *event with* $m_{\rm H}$*=120GeV/c*^{2}*. The photon energies are 62 GeV and 194 GeV.*

The reconstructed mass of the Higgs boson is displayed on Fig. 15. A gaussian fit leads a resolution σ of 2.1 GeV/c^2. 92.3% of the events are in a 3σ region around the 120.0±0.13 GeV/c^2 mean value.

Similar results are obtained with Z decaying in pair of electrons. Figure 16 displays the difference between the simulated mass of the Z and reconstructed one. A resolution of 1.9 GeV/c^2 is observed.

ZZ and WW processes

In order to evaluate the impact of the Si/W calorimeter performances, the ability to reconstruct and separate a pair of Z from a pair of W is tested. The processes under consideration are $e^+e^- \to \nu\bar{\nu}ZZ$ and $e^+e^- \to \nu\bar{\nu}WW$ at a centre-of-mass energy of 800 GeV. The two neutrinos in the final state prohibit any total energy constraint and the interest of such a test is reinforced. A fast simulation reflecting the performances of the calorimeters obtained from GEANT simulations, as described in section 1 is used to perform the analysis. The Energy Flow objects are clustered with DURHAM jet-clustering algorithm [9]. The variation of the y_{cut} is stopped when the transition between three and four jets occurs and therefore the event is forced into a four jets topology. The pairing associated to the smallest difference between the di-jet masses is chosen as the candidate pairing and determines the two di-jet masses : M_{12} and M_{34}. A likelihood estimator combines y_{cut}, M_{12} and M_{34} with the number of b- and c-like jets in the

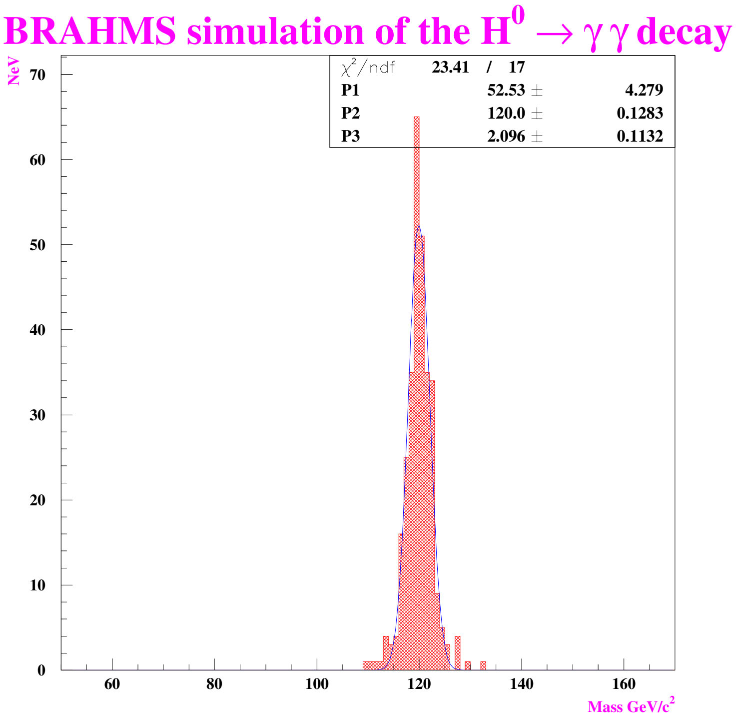

Figure 15: *Reconstructed mass of the $H \rightarrow \gamma\gamma$ decay. The results of a gaussian fit of the mass spectrum is also shown.*

event evaluated from the parametrisation defined in Ref [10].
The Fig. 17 displays the reconstructed di-jet masses for both processes where a very clear discrimination between the Z and the W is observed.

$e^+e^- \rightarrow hhZ$ process

In order to illustrate the impact of the Energy Flow resolution on multi-jets final state, a specific analysis of hhZ leading to the trilinear Higgs coupling measurement is conducted. As described in more details in Ref. [11] part of the discrimination between the signal and the background could be exhibited with the variable DIST defined as $\mathrm{DIST}^2 = (\mathrm{m}_{12} - m_\mathrm{h})^2 + (\mathrm{m}_{34} - m_\mathrm{h})^2 + (\mathrm{m}_{56} - m_\mathrm{Z})^2$, where m_h and m_Z are the Higgs and Z bosons mass respectively, and m_{12}, m_{34}, m_{56} the three reconstructed di-jet masses. This variable is displayed on Figure 18 both for signal and sum of the background processes for two Energy Flow jet resolutions. Another way to look at the impact of the Energy Flow resolution on multi-jet final states is displayed on Fig. 19.The improvement obtained by an Energy Flow resolution less than $35\%/\sqrt{\mathrm{E_{jet}}}$ is clearly observed.

This comparison emphasizes the importance of a very high granularity calorimeter with an excellent coverage.

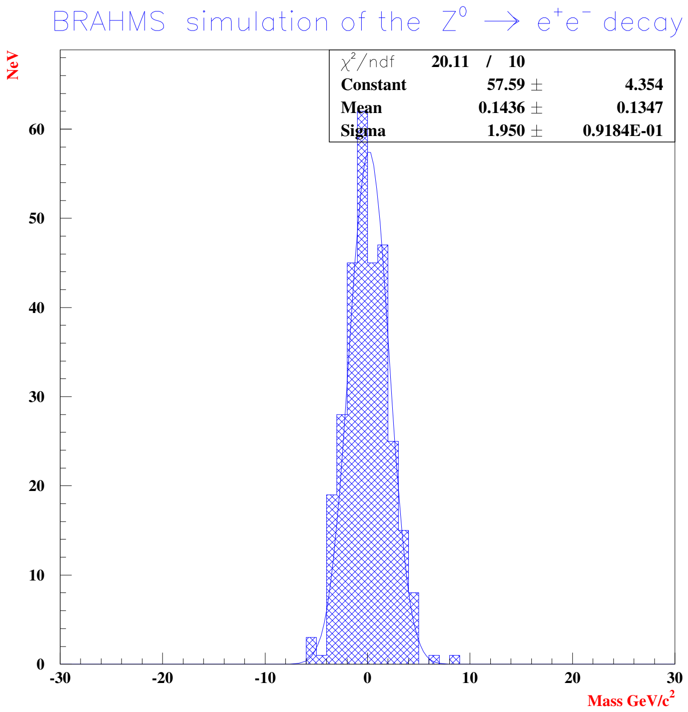

Figure 16: *Difference between the reconstructed mass of the $Z \rightarrow e^+e^-$ decay and simulated mass value of the Z boson. The result of the Gaussian fit of the mass spectrum is also shown.*

9 Conclusions

The studies of the high granularity calorimeters design lead to very good performances with single particles as well as with jet reconstructions. Even in tricky situations, the separation of both photons and neutral hadrons from charged hadrons is shown to be possible.

The multi-jet final states analyses are of major importance in the next Linear Collider Physics and requires excellent jet energy resolution. The high granularity calorimeters are well suited for this purpose; the reconstruction of the jets based on full simulation leads to an energy resolution of $35\%/\sqrt{E_{jet}}$.

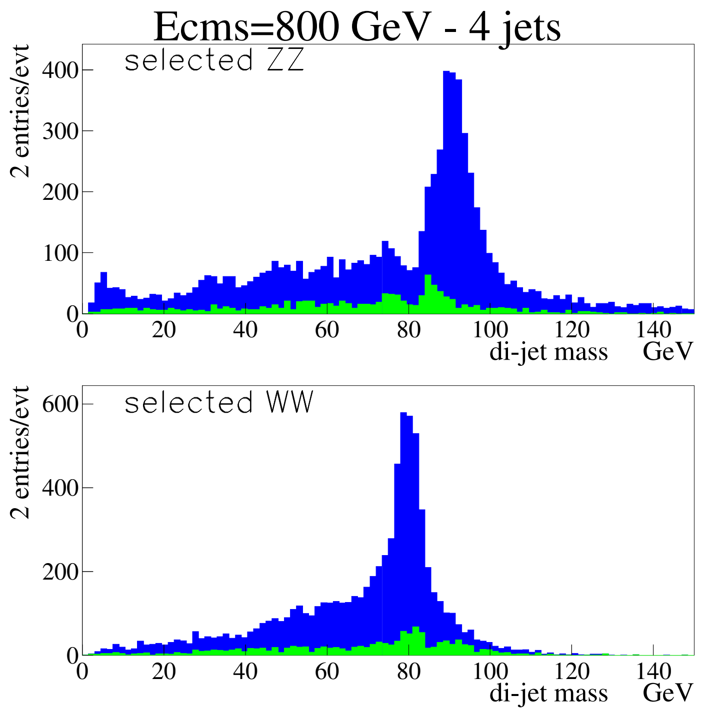

Figure 17: *Reconstructed di-jet mass in (a)* $e^+e^-\to\nu\bar{\nu}ZZ$ *and (b)* $e^+e^-\to\nu\bar{\nu}WW$*. In each case the dark histogram corresponds to signal pairing while the light histograms represents the background processes contribution.*

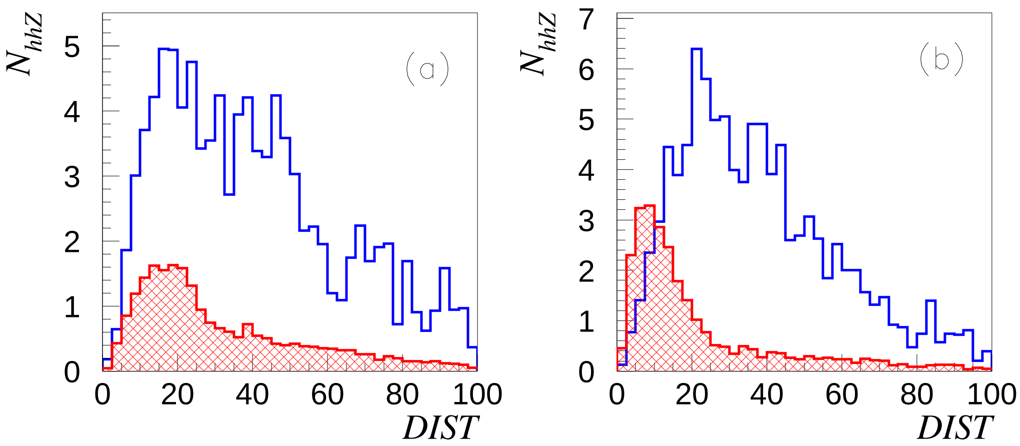

Figure 18: *Distribution of the variable DIST (defined in text) for two* ENERGY FLOW *resolutions: a)* $60\%(1.+|\cos\theta_{\rm jet}|)/\sqrt{\rm E_{jet}}$ *b)* $30\%/\sqrt{\rm E_{jet}}$*. The shaded histogram shows the signal, the solid one displays the sum of the background processes.* $m_{\rm h}$*=120 GeV/c*^{2} *and an integrated luminosity of 1000 fb*$^{-1}$ *are assumed.*

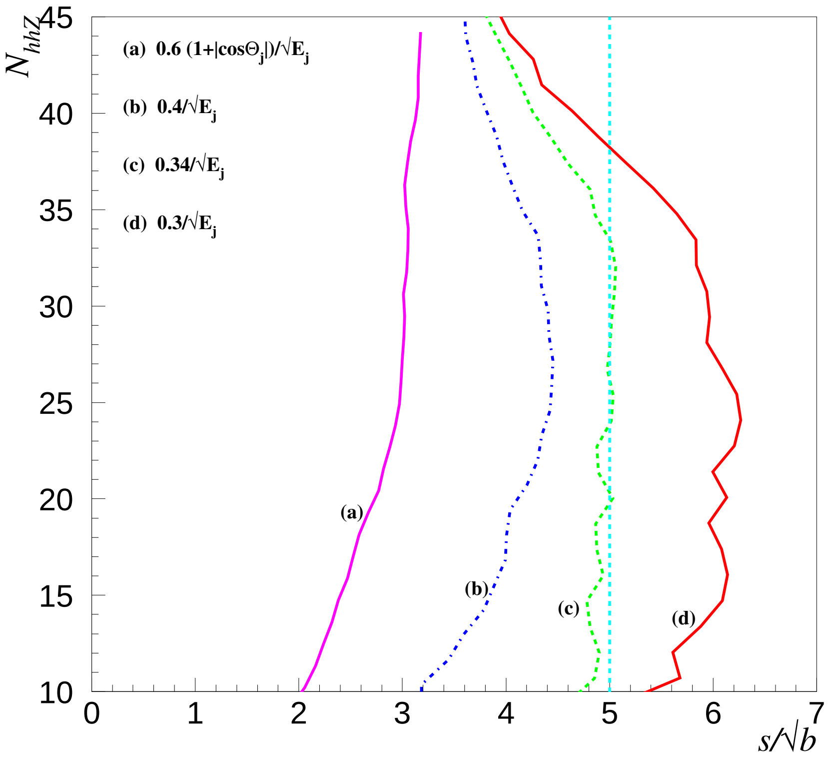

Figure 19: *Number of expected* $e^+e^- \to hhZ \to$ *6 jets as a function of the figure of merit defined as* $s/\sqrt{b}$*, for different choices of* ENERGY FLOW *jet resolutions;* m_h*=120 GeV/c*^{2} *and an integrated luminosity of 1000 fb*$^{-1}$ *have been assumed.*

References

[1] H. Videau, *A W-Si electromagnetic calorimeter for Higgs Physics at a Linear Collider*, talk given in Linear Collider Workshop 2000, Fermi National Accelerator Laboratory, October 24-28, 2000, Batavia, Illinois, USA.

[2] http://wwwinfo.cern.ch/asd/geant4/geant4.html and Refs. herein

[3] P. Mora de Freitas, *Calorimeter studies with GEANT4* , talk given in Linear Collider Workshop 2000, Fermi National Accelerator Laboratory, October 24-28, 2000, Batavia, Illinois, USA.

[4] P. Gay, *Photon Reconstruction Status*, Talk given at ECFA-DESY Linear Collider Workshop, 5-8 May 2000, Padova.

[5] D. Orlando, *Neutral hadron reconstruction*, Talk given at ECFA-DESY Linear Collider Workshop, 5-8 May 2000, Padova.

[6] T. Sjöstrand, High-energy-physics event generation with PYTHIA 5.7 and JETSET 7.4, Compt. Phys. Commun.82 (1994) 74.

[7] G. Blair *et. al* , *An ab initio Monte Carlo*, `http://www.hep.ph.rhbnc.ac.uk/ blair/detsim/brahms.ht` T. Behnke, *A full detector simulation framework for a detector at TESLA*, Talk given at Linear Collider Workshop 2000, Fermi National Accelerator Laboratory, October 24-28, 2000, Batavia, Illinois, USA.

[8] "Geant - Detector Description and Simulation Tool", CERN Program Library Writeup W5013, Application Software Group, Computing and Networks Division, CERN, Geneva, Switzerland; http://wwwinfo.cern.ch/asdoc/geant_html3/geantall.html

[9] W.J. Stirling, Hard QCD Working group-Theory Summary, J.Phys. G17 (1991) 1567

[10] R. Hawkings, Vertex detector and flavour tagging studies for the TESLA linear collider, LC-PHSM/2000-026

[11] C. Castanier *et. al* , Higgs self coupling in e^+e^- collisions, LC-Note/2001 *in preparation*; P. Gay, *Higgs self-couplings at* $\sqrt{s}$*=500 GeV*, talk given in Linear Collider Workshop 2000, Fermi National Accelerator Laboratory, October 24-28, 2000, Batavia, Illinois, USA